Rock physics modeling of shale during smectite-to-illite transition

Xuan Qin, De-hua Han, and Fuyong Yan, Rock Physics Lab, University of Houston*

Summary

It is essential to quantitatively study how shale properties change during smectite-to-illite transition, which can assist us to better predict pore pressure and understand the shale diagenesis. We develop rock physics models to characterize how elastic stiffness and porosity of shale change during this transition. The bound water bulk and shear moduli are inverted at around 9.7 and 2 GPa with effective medium theory based on the results of molecular dynamics. With two bulk volume models, we simulate the velocity and density variations for two separate cases of smectite-to-illite, fluid expansion and fluid loss. Pore pressure increase can be resolved for fluid expansion. Our modeling results suggest that velocities can decrease by 8%, density changes little, and Vp/Vs ratio increases by 15% if fluid expansion happens and velocities increase by 5%, Vp/Vs ratio decreases by 4% if fluid loss takes place.

Introduction

Smectite-to-illite (S-to-I) is a vital mechanism to cause high magnitude overpressure (Lahann et al., 2001; Katahara, 2003; Yu and Hilterman, 2014). People have several choices when performing pore pressure prediction for shales containing such diagenesis, e.g. shale compaction model by Dutta (1986), elastic unloading method by Bowers (1995), and load transfer method by Lahann et al. (2001). Most of these study are empirical and can work with local calibration. However, little work has focused on shale's microstructure and quantitative description of how shale's elastic stiffness along with pore pressure change during the transition.

Qin and Han (2016) categorized two trends of S-to-I, based on the sonic travel time and density crossplot. During the transition, if bound water in smectite transfers to free water and is preserved in the pore system, fluid expansion (Figure 1a) causes more velocity decrease and little density change as well as high magnitude overpressure. If the released water can escape, shale has more density increase and little velocity change with relatively low pore pressure increase.

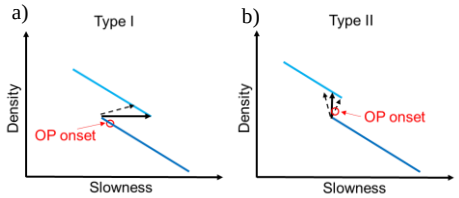

Figure 1. Sketches of two trends of smectite-to-illite: a) trend I and b) trend II. The solid arrows denote the end-member cases of fluid expansion and fluid loss. The dashed arrows denote some possible mixed cases. Modified from Qin and Han (2016).

Since this diagenesis involves transferring bound water to free water, we determine the bound water properties from molecular dynamics study (Ebrahimi et al., 2012) to emulate the stiffness of smectite with varying amounts of bound water. Then we employ anisotropic differential effective medium (ADEM) method to model shale stiffness with two bulk volume models corresponding to fluid expansion and fluid loss respectively. The modeling elastic properties and densities resemble the trends by Qin and Han (2016). Pore pressure increase during this transition can be resolved with the proposed model.

Smectite group of clay and bound water

Clay minerals have sheet-like or layered structure, consisting of two basic unit: the silicon tetrahedral sheet (T) and alumina octahedral sheet (O). Clay minerals composed of a three-layered structure (T-O-T) belong to the smectite group. Smectite and illite are quite common in the group. In illite, the distance between the first silica layer of one T-O-T sheet and the next silica layer of neighboring T-O-T sheet (basal spacing) is about 10 Å (Figure 2). The basal spacing of smectite is around 15 Å, but can shift between 9 Å to 21 Å, resulting from smectite adsorbing various amounts of polar water molecules present in between the clay platelets. These water is called bound or interlayer water, which is part of clay particles and can be eliminated between 110 and 200 °C in lab. The diameter of a water molecule is close to 3 Å, basal spacing with 1, 2, and 3 layers of bound water are 12, 15, and 17.8 Å, respectively (Ebrahimi et al., 2012).

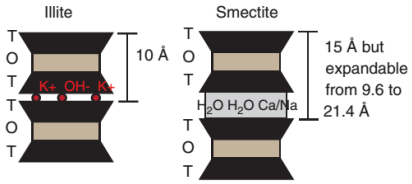

Figure 2. Smectite group of clay minerals with T-O-T structure: (left) illite and (right) smectite sheet and bound/interlayer water. Modified from Moyano et al. (2012).

The amount of clay bound water ϕ_{bw} is determined by the following equation (Hill et al., 1979)

$$\phi_{bw} = \phi_t \cdot SF \cdot Qv\,, \qquad (1)$$

where ϕ_t is total porosity, SF is salinity factor and Qv is the Cation Exchange Capacity (CEC) in the unit of meq/ml pore space. SF is calculated with salinity S in g/L through

$$SF = 0.6425 \cdot S^{-0.5} + 0.22, \quad (2)$$

Therefore, clay bound water content will decrease with increasing salinity or decreasing CEC. For example, smectite typically has CEC ranging from 0.6 to 1 meq/ml, comparing with CEC of illite ranging from 0.1 to 0.4 meq/ml. So smectite is more expandable than illite. As the salinity of formation water can vary between 1 and 400 g/L, the ratio of bound water to total porosity is usually less than 0.4, which can constrain our rock physics modeling.

Smectite-to-illite (Lahann and Swarbrick, 2011; Yu and Hilterman, 2014) comes up in shale at a temperature above 70 °C. The reaction mechanism (Boles and Franks, 1979) can be represented with the following expression,

$$\text{Smectite+K-feldspar} \rightarrow \text{Illite+Quartz+n}H_2O\cdot$$

Smectite reacts with potassium ion from K-feldspar to form illite and cemented quartz and expels extra amounts of intergranular water.

Methodology

Modeling smectite mineral properties

Modeling the smectite mineral properties is significant due to the feature of dehydration. Because changes of bulk volume, density and modulus from K-feldspar to quartz is smaller than those changes from smectite to illite and water, we presume that smectite mineral can be seen as composed of illite sheet and soft interlayer or bound water. Hence, the interlayer thickness will decreases during S-to-I transition. The bound water elastic properties are determined with the following part.

The largest difference between bound water and free water is that bound water cannot move freely in the pore space instead of being adsorbed by the charged clay minerals. To characterize this, several authors (Holt and Fjær, 2003; Kolstø and Holt, 2013) set non-zero shear modulus when they modeled the elastic properties of shale. By using discrete particle flow model, the shear stiffness of the clay interlayer region increases from zero to a few GPa when clay surface are charged (Kolstø and Holt, 2013).

The elastic properties of Na-montmorillonite as a function of hydrated status have been calculated by Ebrahimi et al. (2012). They obtain the full elastic tensor of Na-montmorillonite with 0 to 258 water molecules added into the interlayer by using molecular dynamics with a force-field for structural simulation of clay minerals. 0 to 258 water molecules make the basal spacing range from 9.3 to 19.5 Å. Due to such a tiny thickness comparing with seismic or ultrasonic wavelength, if we treat the smectite with various thickness of bound/interlayer water as a two-phase medium, we can use Backus average (Backus, 1962) to invert the bound water properties for each basal layering spacing.

We approximate the general elastic tensor of Na-montmorillonite with 21 elastic constants to a transverse isotropic (TI) medium with 5 elastic constants through an algorithm by Dellinger (2005). Since we have known the elastic stiffness and basal layer spacing (Å) of Na-montmorillonite without and with up to 258 water molecules, we can calculate the elastic stiffness of a two-phase medium comprised of dry clay and bound water by given a series values of bulk (2.5 to 15 GPa) and shear moduli (0 to 22.5 GPa) of bound water. By seeking the minimum error defined by the following expression,

$$e = \sqrt{\sum_{ij}\left(\frac{c_{ij} - C_{ij}}{C_{ij}}\right)^2}, \quad (3)$$

where c_{ij} represents the modeling results of c_{11}, c_{33}, c_{44}, and c_{66}, and C_{ij} denotes the corresponding stiffness approximated from Ebrahimi et al. (2012), we can determine the best fit values of bulk and shear moduli of bound water at each individual basal spacing (Figure 3).

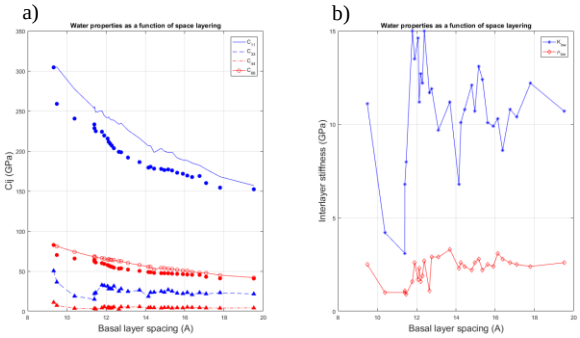

Figure 3. a) Modeling stiffness and approximated data for Na-montmorillonite as a TI medium vary with basal spacing. Blue circles, blue triangles, red circles, and red triangles denote modeling results of c_{11}, c_{33}, c_{44}, and c_{66}; blue solid lines, blue dashed lines, red dash dotted lines, and red lines with circles denote approximated data of C_{11}, C_{33}, C_{44}, and C_{66} from Ebrahimi et al. (2012); b) best fitting results of interlayer stiffness, blue and red color represent bulk and shear moduli of interlayer (bound water) as a function of basal layer spacing Å.

From the modeling results, we can observe that the bound water moduli as a function of basal spacing is not monotonous but fluctuate around 10 GPa and 2 GPa for bulk and shear moduli. From figures 3a and 4, we notice that C_{11} and C_{66} are totally underestimated (can be as high as 15%), which reflects the deficiency when we use Backus

average to model horizontal stiffness of smectite. C_{33} and C_{44} have tiny errors less than 1% and 5%, which gains our confidence when characterizing vertical stiffness of smectite. Hereby, we do not utilize and model C_{13} because it usually has larger uncertainty than other elastic constants.

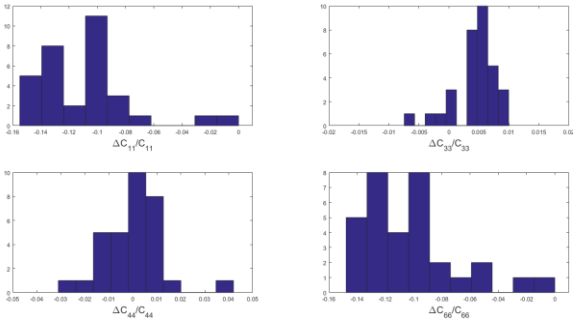

Figure 4. Error statistics for C_{11}, C_{33}, C_{44}, C_{66}. The horizontal axis represents the relative change between modeling results and approximated data from Ebrahimi et al. (2012). The vertical axis represents frequency.

Because of the fluctuation and narrow range of inverted bulk and shear moduli of bound water, we run another test to see what values they will be if we set elastic properties of bound water as invariants. By minimizing the sum of errors at all of the basal spacing,

$$e = \sqrt{\sum_{ij}\sum_{l}\left(\frac{c_{ij}-C_{ij}}{C_{ij}}\right)^2}, \qquad (4)$$

where l represents each of the basal spacing, the best fitting results of bulk and shear moduli for bound water is 9.7 and 2 GPa. With these values, modeling results of smectite stiffness resemble Figure 3a, in spite of larger errors between 9.5 and 11.5 Å, due to the effects of first a few water molecules on stiffness.

Bound water density will exceed 1 g/cc, when smectite platelet has a basal spacing less than 20 Å (Colten-Bradley, 1987). Its density can vary from 1.02 to 1.15 g/cc for different numbers (up to 3) of water layers being adsorbed. We apply it as 1.1 g/cc in our modeling.

Modeling shale stiffness during smectite-to-illite

In our shale rock physics modeling, we use dry sheet illite-smectite elastic stiffness derived from first-principle calculations and density function theory by Militzer et al. (2011). We combine these dry sheet illite-smectite elastic constants (C_{11}, C_{33}, C_{44}, C_{66}, and C_{13} are 83.6, 49, 22.6, 31.5, and 19.3 GPa, respectively) with the bulk and shear moduli of bound water to simulate elastic stiffness of smectite with various interlayer thickness of bound water as a TI medium. We use Anisotropic Differential Effective Medium (ADEM) method (Nishizawa, 1982) to simulate shale elastic properties. This is because DEM treats each constituent asymmetrically. To preserve the features of connectivity and load-bearing material, we use smectite as host material and add pores filled with free water as inclusions, which have ellipsoid shape with an aspect ratio of 0.6. The bulk modulus and density of water are determined from FLAG program of Fluids/DHI consortium by setting a temperature of 80 °C and a pressure of 30 MPa.

Our modeled clay mineral properties is at clay platelet scale, which has a symmetry vertical to the shale bedding. However, the clay aggregates vary in orientation but aligned locally, and a considerable portion of clay particles are randomly oriented. In general, the degree of alignment presents a wide range of dispersion and depends on the compaction and geological history (Hornby et al., 1994). To compute the stiffness of an aggregate of partially aligned domains, we can average the elastic properties by using the orientation distribution function (ODF) suggested by Dræge et al. (2006), which can be expressed as a function of quartz content and porosity. Alternatively, ODF can also be obtained via Scanning Electron Microscope (SEM) image.

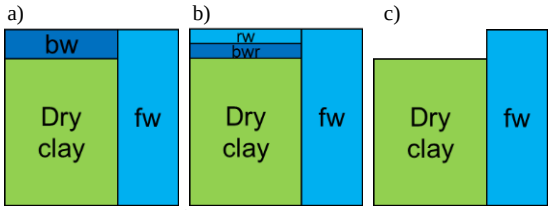

Figure 5. Schematic of bulk volume model used in our shale rock physics modeling: a) original status, b) fluid expansion, and c) fluid loss; "bw, "rw", "bwr", and "fw" represent bound water, released water from bound water, remained bound water, and free water.

Figure 5 illustrates the bulk volume models we use. Initially, as in Figure 5a, the shale consists of pores filled with water and solid phase, smectite clays composed of dry clay and bound water. When the environment, such as temperature and pressure satisfy, S-to-I occurs and releases bound water and transfers it to free water. If the released water (denoted with "rw" in Figure 5b) does not drain and is totally preserved in the pores, solid part dissolves and leaves a void that resembles a crack. The surrounding grains will tend to collapse into the void, and thereby compress the pore water as well as increasing pore pressure. Additionally, as free water density is less than bound water and the volume of the system remains, released water will induce pressure increase, which can be calculated through

$$\Delta P = -K_w\left(\frac{\rho_w}{\rho_{bw}}-1\right), \qquad (5)$$

where K_w, ρ_w, and ρ_{bw} represent water bulk moduli, water density and bound water density. The above load transfer process can be modeled as a result of crack opening and pore pressure increase. We decrease the volume of bound water and add the identical volume of soft pores with an aspect ratio of 0.01 as inclusions.

Fluid loss is another case in Figure 5c. During the transition, the released bound water is able to fully escape, so porosity decreases and bulk density increases. As fluid density does not change, no internal pore pressure generates and the effective stress remains and velocity may change trivially.

Moreover, Ho et al. (1999) and Carpentier et al. (2003) observed the alignment of clay minerals is progressively enhanced within a narrow depth corresponding to smectite-to-illite zone. Because fluid expansion does not involve bulk volume change, we assume clay minerals alignment degree unchanged. While fluid loss leads to continuing compaction, the clay minerals become more aligned in this case. Therefore, the orientation distribution is related with total pore space, which is the sum of pores filled with free water and interlayer space filled with bound water.

Rock physics modeling results

Figure 6a and 6b represent our modeling velocities of fluid expansion and fluid loss, respectively. The initial interlayer spacing of smectite platelet is set as 7 Å, and can decrease to 1 Å, which simulates the process of bound water transferring to free water.

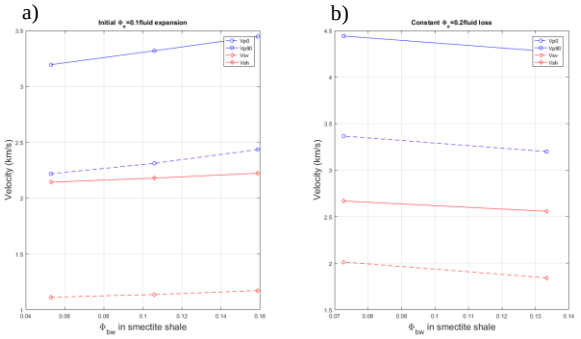

Figure 6. Rock physics modeling of velocities against bound water porosity during smectite-to-illite for a) fluid expansion and b) fluid loss. Blue solid and dashed lines with circles represent P-wave velocity propagating parallel and normal to the bedding direction; red solid and dashed lines with diamonds represent SH-wave velocity propagating and polarizing in the bedding and SV-wave propagating or polarizing normal to the bedding.

For fluid expansion case (Figure 6a), it has an initial mechanical porosity of 10%. Constrained by $\phi_{bw} / \phi_t <$ 0.4, the interlayer spacing can vary from 1 to 3 Å, corresponding to the three calculated bound water porosity ϕ_{bw} in the horizontal axis. When the bound water porosity decreases, transferred free water open cracks, and thus velocities decrease from left to right. Density changes little since no fluid loss.

Figure 6b simulate fluid loss case of smectite-to-illite with a constant mechanical porosity of 20%. Two calculated data for each velocity corresponds to interlayer spacing varying from 1 to 2 Å or bound water porosity varying from 7 to 13.5%. In this case, bound water escapes out of the system, so the total porosity decreases and velocities increases.

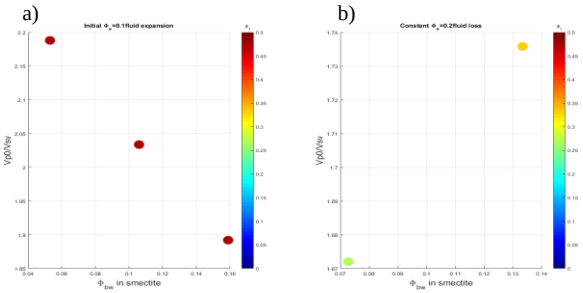

Figure 7. Rock physics modeling of vertical Vp/Vs ratio varying with bound water porosity during smectite-to-illite for a) fluid expansion and b) fluid loss. Total porosity is color-coded.

Figure 7a displays the Vp/Vs ratios increase with the decrease of bound water porosity during fluid expansion. This is because the bound water with shear rigidity transfers to free water without shear rigidity. For fluid loss in figure 7b, the Vp/Vs ratios decrease with the bound water content. This continuing compaction reflects a compaction feature (increase of Vp/Vs) of clastic sediments.

Conclusions

After modeling smectite mineral elastic stiffness varying with bound water content, we devise workflows to quantify shale elastic properties during smectite-to-illite. Modeling results suggests that decrease of velocities and increase of pore pressure are the results of fluid expansion. Continuing compaction will occur if the released bound water totally drains for the fluid escape case. Future work will build rock physics templates to combine these two scenarios and describe how stiffness and pressure change if bound water partially escapes.

Acknowledgements

The authors would like to thank Fluids/DHI consortium for finical support. We also appreciate Davoud Ebrahimi for use of his calculated data of Na-montmorillonite with various basal spacing.

EDITED REFERENCES

Note: This reference list is a copyedited version of the reference list submitted by the author. Reference lists for the 2016 SEG Technical Program Expanded Abstracts have been copyedited so that references provided with the online metadata for each paper will achieve a high degree of linking to cited sources that appear on the Web.

REFERENCES

Backus, G., 1962, Long-wave elastic anisotropy produced by horizontal layering: Journal of Geophysical Research, **67**, 4427–4440, http://dx.doi.org/10.1029/JZ067i011p04427.

Boles, J. R., and S. G. Franks, 1979, Clay diagenesis in Wilcox sandstones of southwest Texas: implications of smectite diagenesis on sandstone cementation: Journal of Sedimentary Research, **49**, 55–70, http://dx.doi.org/10.1306/212F76BC-2B24-11D7-8648000102C1865D.

Bowers, G. L., 1995, Pore pressure estimation from velocity data: Accounting for overpressure mechanisms besides undercompactions: SPE Drilling and Completion, **10**, 89–95.

Charpentier, D., R. H. Worden, C. G. Dillon, and A. C. Aplin, 2003, Fabric development and the smectite to illite transition in Gulf of Mexico mudstones: An image analysis approach: Journal of Geochemical Exploration, **78**, 459–463.

Colten-Bradley, V. A., 1987, Role of pressure in smectite dehydration: Effects on geopressure and smectite-to-illite transformation: AAPG Bulletin, **71**, 1414–1427.

Dellinger, J., 2005, Computing the optimal transverse isotropic approximation of a general elastic tensor: Geophysics, **70**, no. 5, I1–I10, http://dx.doi.org/ 10.1190/1.2073890.

Dræge, A., M. Jakobsen, and T. A. Johansen, 2006, Rock physics modeling of shale diagenesis: Petroleum Geoscience, **12**, 49–57, http://dx.doi.org/10.1144/1354-079305-665.

Dutta, N. C., 1986, Shale compaction, burial diagenesis, and geopressures: A dynamic model, solution and some results, *in* J. Burrus, ed., Thermal modeling in sedimentary basins: Editions Technip, 149–172.

Ebrahimi, D., R.J.M. Pellenq, and A.J. Whittle, 2012, Nanoscale elastic properties of montmorillonite upon water adsorption: Langmuir, **28**, 16855–16863.

Hill, H. J., G. E. Klein, O. J. Shirley, E. C. Thomas, and W. H. Waxman, 1979, Bound water in shaly sands-Its relation to Q and other formation properties: The Log Analyst, **20**, 3–19.

Ho, N., D. R. Peacor, and B. A. van der Pluijm, 1999, Preferred orientation of phyllosilicates in Gulf Coast mudstone and relation to the smectite-illite transition: Clays and Clay Minerals, **47**, 495–504.

Holt, R.M., and E. Fjær, 2003, Wave velocities in shale: A rock physics model: 65th Annual International Conference and Exhibition, EAGE, Extended Abstracts.

Hornby, B. E., L. M. Schwartz, and J. A. Hudson, 1994, Anisotropic effective-medium modeling of the elastic properties of shales: Geophysics, **59**, 1570–1583, http://dx.doi.org/10.1190/1.3513265.

Kataraha, K., 2003, Analysis of overpressure on the Gulf of Mexico shelf: OTC, 15293.

Kolstø, M., and R. M. Holt, 2013, Bound water in clay and shale and its influence on P- and S-wave velocities: The 2nd International Workshop on Rock Physics.

Lahann, R. W., D. K. McCarty, and J. C. C. Hsieh, 2001, Influence of clay diagenesis on shale velocities and fluid-pressure: OTC, 13046.

Lahann, R. W., and R. E. Swarbrick, 2011, Overpressure generation by load transfer following shale framework weakening due to smectite diagenesis: Geofluids, **11**, 362–365.

Militzer, B., H.-R. Wenk, S. Stackhouse, and L. Stixrude, 2011, First-principles calculation of the elastic moduli of sheet silicates and their application to shale anisotropy: American Mineralogist, **96**, 125–137.

Moyano, B., K. T. Spikes, T. A. Johansen, and N. H. Mondol, 2012, Modeling compaction effects on the elastic properties of clay-water composites: Geophysics, **77**, no.5, D171–D183, http://dx.doi.org/10.1190/GEO2011-0426.1.

Nishizawa, O., 1982, Seismic velocity anisotropy in a medium containing oriented cracks: Journal of Physics of the Earth, **30**, 331–347.

Qin, X., and D. Han, 2016, Seismic characters of pore pressure due to Smectite-to-illite transition: 78th Annual International Conference and Exhibition, EAGE, Extended Abstracts.

Yu, H., and F. J. Hilterman, 2014, The effect of pressure on rock properties in the Gulf of Mexico: comparison between compaction disequilibrium and unloading, Interpretation, **2**, SB1–SB15.